Epitaxial growth of ultrathin Cr films on Mo(110) at elevated temperature

A. Cazacu,* S. Murphy, and I. V. Shvets
SFI Laboratory, School of Physics, Trinity College, University of Dublin, Dublin 2, Ireland
(Received 2 August 2005; revised manuscript received 1 December 2005; published 13 January 2006)

The principal details of Cr film growth on Mo(110) at elevated temperature are described. Cr films form nanostripes by the step-flow growth mechanism for film coverages up to 3 monolayers. In contrast to the Fe/Mo(110) system, there is no indication of strain relaxation in either the first, second, or third layers. The Cr nanostripes remain pseudomorphic up to the onset of Stranski-Krastanov growth, which is typified by the formation of nanowedge islands. This is accompanied by the formation of a two-dimensional dislocation network within the nanowedge islands. Two types of steps can be observed on top of the Cr nanowedges, unlike the Fe/Mo(110) system where the (110) surface of the Fe nanowedges is unbroken by any steps. The first are monatomic steps formed by incomplete Cr layers, while the second are fractional steps formed between adjacent layers with different degrees of tetragonal distortion. The fractional steps are modeled using the first principles calculations.

DOI: 10.1103/PhysRevB.73.045413 PACS number(s): 68.55.Ac, 68.55.Jk

I. INTRODUCTION

There has been much interest in the growth of magnetic epitaxial overlayers on refractory metal substrates with respect to the effects of interfacial electron transfer and large lattice mismatch on the magnetic properties of the overlayer. Also, because of their relatively high surface energies, refractory metal substrates offer the possibility of growing wetting layers with little interdiffusion over a wide temperature range. Scanning tunneling microscopy (STM) and low-energy electron diffraction (LEED) provide useful tools for gathering information on the structural properties of the interface and on the progression of film morphology under different growth conditions.

While ferromagnetic overlayers such as Fe/W,[1,2] Fe/Mo,[3,4] Ni/W,[5] Co/W,[6,7] and Co/Mo (Ref. 8) have been well-studied, less is known about the growth and properties of Cr overlayers on refractory metals. The growth of Cr on W(110) and W(100) has previously been studied by field electron emission microscopy (FEEM), Auger electron spectrsocopy (AES), LEED, and temperature programmed desorption (TPD).[9,10] It was found that a (1×1) pseudomorphic monolayer (ML) is formed on W(110) at 100 K, which is thermally stable up to the Cr desorption temperature of 1290 K. A Cr bilayer on W(110) is thermally stable up to 800 K, whereupon three-dimensional islands are formed. Between 500 and 800 K the bilayer displays a (2×2) LEED pattern. Multilayer films with coverages greater than 2 ML form three-dimensional islands supported on a Cr bilayer between 400 and 800 K, and on a Cr monolayer above 800 K. The multilayer films are characterized by the presence of a (11×11) coincidence lattice, similar to that observed by Gradmann and Waller for the Fe/W(110) epitaxial system.[11] To our knowledge, STM studies of the Cr/W(110) epitaxial system have been limited to the observation of anisotropic submonolayer growth at room temperature.[12] Comparison of the Mo/Cr/Mo(001) and vacuum/Cr/Mo(001) interfaces, using first principles density-functional theory (DFT) calculations, has indicated that the bare Cr/Mo(001) interface exhibits spin-polarized behavior, but that the magnetism is totally quenched up to 35 ML by the presence of a single Mo capping layer.[13] Experimentally, Cr coated W tips have been employed to perform spin-polarized STM (SP-STM) measurements of Fe bilayers on W(110).[14]

In this paper, STM and LEED were used to investigate the growth and morphology of Cr films on the Mo(110) surface at elevated temperatures. The Cr/Mo(110) system is similar in terms of symmetry, misfit $(a_{\mathrm{Mo}}-a_{\mathrm{Cr}})/a_{\mathrm{Cr}}=8.4\%$, and surface free energies ($\gamma_{\mathrm{Cr}}=2.3$ J m^{-2}, $\gamma_{\mathrm{Mo}}=3.0$ J m^{-2})[15] to the widely studied Fe/W(110) and Fe/Mo(110) systems. However, Cr/Mo(110) has not been previously studied by STM and we will highlight some key differences between these systems. First principles DFT calculations have been applied to compare the Cr/Mo(110) and Fe/Mo(110) interfaces in order to explain these differences.

II. EXPERIMENT

The sample preparation and analysis were performed in an ultrahigh vacuum (UHV) multichamber system with a base pressure in the low 10^{-10} mbar range. The Mo(110) substrate was prepared from a 4N purity single crystal with a miscut angle of 0.4° off the (110) plane, which yielded an average terrace width of the order of 32 nm. The terraces were separated by monatomic steps 2.1 Å in height, which were oriented along the $[\bar{1}11]$ direction. The substrate was cleaned by alternate cycles of oxidation and flash annealing. The surface was first oxidized by annealing at 1600 ± 100 K in a 7×10^{-7} mbar O_2 atmosphere for 90 min. The resulting oxide was removed from the surface by repeated flash annealing to 2300 ± 100 K for 20 s cycles in UHV. This procedure was repeated until the carbon and oxygen impurity levels were below the detection limit of the Auger electron spectroscopy (AES) setup. The clean surface gave a sharp 1×1 LEED pattern. Typically, the sample was cleaned about 1 h before each evaporation. The sample temperature during deposition was measured by a K-type thermocouple attached

near the sample, giving an estimated accuracy in the temperature of ±50 K. Cr films were deposited using electron beam evaporation of 99.9% purity Cr from a highly oriented pyrolitic graphite crucible. The chamber pressure did not rise above 3.5×10^{-10} mbar during evaporation. Film coverages θ are described in pseudomorphic monolayers (ML), where $\theta=1$ for 1.43×10^{19} Cr atoms m^{-2}, which corresponds to the atomic packing density of a Mo(110) crystal plane. The deposition rate was monitored by a quartz crystal balance and was kept constant at 0.27 ML/min for all the depositions. Coverages were determined from the deposition flux measured by the quartz crystal balance or directly from the STM data where this was possible. STM was performed at room temperature, in constant current mode, using W tips and a typical tunnel current of $I_t=0.1$ nA and bias $V=30$ mV.

The calculations were performed using the CASTEP program[16] as a module of Materials Studio. We have considered five vacuum slabs: (i) a 7 ML Mo(110) substrate, (ii) 1 ML Cr on a 5 ML Mo(110) substrate, (iii) 2 ML Cr on 5 ML Mo(110), (iv) 1 ML Fe on 5 ML Mo(110), and (v) 2 ML Fe on 5 ML Mo(110). The slabs are constrained in-plane to the substrate lattice parameter to reproduce the experimentally observed pseudomorphic growth. The general gradient approximation (GGA) using the local Perdew-Burke-Ernzerhof (PBE) functional[17] was used to optimize the interlayer separations within each slab.

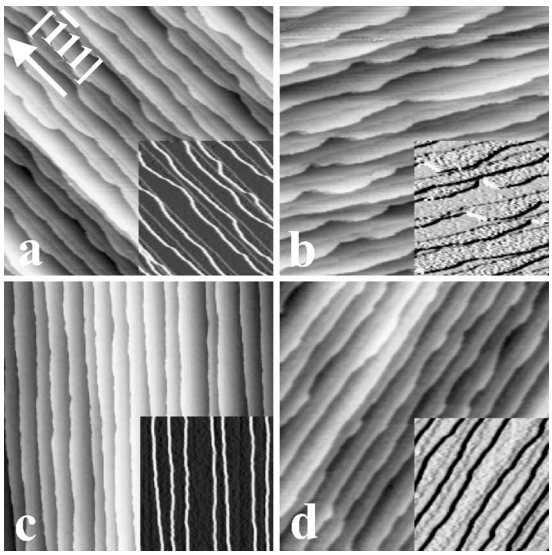

FIG. 1. Topographic STM images of Cr nanostripes formed by step-flow growth on Mo(110) at 575 K. The lower right quadrant of each image shows the differentiated image to enhance contrast. The most intense lines correspond to monatomic steps, while fainter lines correspond to fractional steps. (a) 400×400 nm^2, 0.3 ML coverage, (b) 150×150 nm^2, 0.6 ML coverage, (c) 200×200 nm^2, 2 ML coverage—no fractional steps here, and (d) 300×300 nm^2, 2.3 ML.

III. RESULTS AND DISCUSSION

For film coverages up to 3 ML, Cr films form nanostripes by the step-flow growth mechanism at 575 K, like those shown in Fig. 1. The corresponding LEED patterns are consistent with pseudomorphic growth of the Cr films. The step-flow growth mechanism is obtained in conditions of high substrate temperature and low deposition flux. Adatoms arriving on the Mo surface diffuse until they are incorporated at ascending step edges, causing them to propagate outwards along the miscut direction. The Mo(110) substrate step edges in Fig. 1 are uniformly straight due to the high anneal temperature used during the cleaning procedure. By contrast, the Cr nanostripes display a meandering step front as a result of a morphological instability described by Bales and Zangwill.[18] The instability arises because of a difference in adatom attachment probabilities between ascending and descending step edges caused by the presence of an Ehrlich-Schwoebel barrier at the step edge.[19,20] Under the condition that there is limited adatom diffusion along the step edge, this gives rise to a meandering of the growing step front and eventually leads to the complete breakdown of the step-flow growth. For high terrace coverages, where the nanostripes reach the position of a buried substrate step, their outer edge straightens and follows the line of the buried step. Interstep repulsions of the type described by Li *et al.*[21] may explain why the nanostripes straighten when they reach the position of a buried substrate step edge. However, this may also be the result of a further diffusion barrier due to a change in adatom binding energy across the buried step. This barrier might originate from a loss of adatom coordination, since the buried substrate step edges are distinguished in the STM data by the presence of a sizeable fractional step.

For a 0.3 ML Cr film, the fractional step height between the Mo substrate and the first Cr layer was measured to be 0.35 Å [Fig. 2(a)]. At 1.2 ML coverage, the fractional step between the first and second Cr layers was measured to be 0.28 Å, while for a 2.4 ML coverage, the fractional step between the second and third Cr layers was found to be 0.32 Å. Similar steps have also been observed by STM in the Fe/Mo(110) and Fe/W(110) systems.[4,22,23] To understand the origins of the fractional steps, we have performed density functional theory calculations for the Cr/Mo(110) and Fe/Mo(110) epitaxial interfaces. The calculated values for the interlayer separations are listed in Table I for the vacuum slabs considered. The surface interlayer separation calculated for the bare 7 ML Mo slab is $d_{S(\mathrm{Mo})}=2.133$ Å, which is 4.1% lower than the bulk Mo interlayer separation. This value is close to the value of 2.0 Å that we have measured by STM and compares well with values of 2.14 and 2.19 Å determined experimentally by LEED[24,25] and with a value of 2.131 Å calculated for a 5 ML Mo(110) slab, using the full-potential linearized augmented plane-wave (FP-LAPW) method.[26]

For the 1 ML Cr/Mo(110) slab the interlayer separation at the Cr-Mo interface was calculated to be $d_{S(1\ \mathrm{ML})}=1.887$ Å, which represents a sizeable contraction (8.4%) with respect to the bulk Cr value. Deeper layers of the slab show a slight expansion of the Mo-Mo interlayer separation over the bulk Mo value. For the 2 ML Cr/Mo(110) slab, the contraction of the surface layer is more pronounced at $d_{S(2\ \mathrm{ML})}=1.609$ Å. The interlayer separation at the Cr-Mo interface is slightly

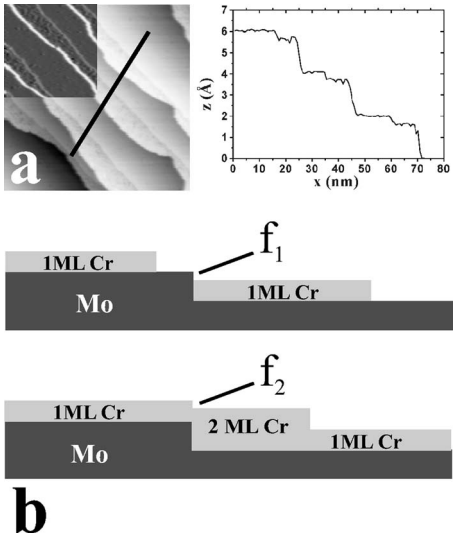

FIG. 2. (a) 100×100 nm^2 STM image of a 0.3 ML Cr film grown on Mo(110) at 575 K. The 0.35 Å fractional step between the Cr layer and the Mo substrate is visible in the line profile. (b) Schematic illustration of the two fractional steps f_1 and f_2. f_1 is the fractional step between the first Cr layer and the bare Mo substrate, obtained at submonolayer coverages. f_2 is the fractional step between the first and second Cr layers, obtained at sesquilayer coverages.

expanded at $d_{S-1(2\ \mathrm{ML})}=2.107$ Å, suggesting that the addition of a second Cr layer reduces the interfacial bonding. Using the values from Table I, the fractional step between the first Cr layer and the substrate as illustrated in Fig. 2(b) was calculated to be $f_1=d_{S(\mathrm{Mo})}-d_{S(1\ \mathrm{ML})}=0.246$ Å, while the fractional step between the first and second Cr layers was calculated to be $f_2=d_{S(\mathrm{Mo})}+d_{S(1\ \mathrm{ML})}-d_{S(2\ \mathrm{ML})}-d_{S-1(2\ \mathrm{ML})}=0.304$ Å. It is expected that a 3 ML Cr/Mo(110) slab will further undergo multilayer relaxations which would result in a difference between fractional steps f_3 and f_2. The 1 ML Fe/Mo(110) and 2 ML Fe/Mo(110) slabs show similar behavior, with contractions of the surface layers and a slight expansion of the Mo-Mo interlayer separations further down in the slab. From the values listed in Table I, fractional steps of $f_1=0.332$ Å and $f_2=0.476$ Å were determined. This compares with an experimental value of around 0.3 Å for both f_1 and f_2, as measured by STM.[4,22] It should be noted that for both the 1 ML Fe/Mo(110) and 2 ML Fe/Mo(110) slabs, the contraction of the surface interlayer separation shown in Table I is larger than the corresponding value calculated by Qian *et al.* using the FP-LAPW method.[26]

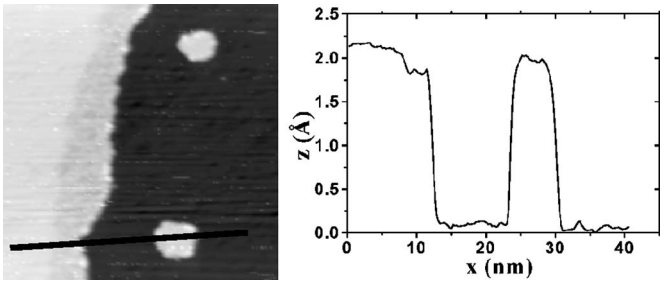

FIG. 3. 43×43 nm^2 STM image of a 0.15 ML Cr film grown on Mo(110) at 500 K. Both islands and a nanostripe are present on the substrate terrace. The difference in height between the islands and the nanostripe is evident in the line profile. The height of the nanostripe was measured to be 1.8 Å, while the island was measured to be 2.0 Å high.

It is also worth noting that the above calculations do not take into account any in-plane strain relaxation, which will reduce the contraction of the surface interlayer separation. In-plane relaxation can occur through the relaxation of adatom positions along the free edges of the Cr nanostripes. Clearly, the level of in-plane relaxation should be higher in free-standing Cr islands than in Cr nanostripes, since the latter remain confined along the edge they share with the substrate steps. This is illustrated in Fig. 3, which shows a 0.15 ML Cr film grown on Mo(110) at the slightly lower temperature of 500 K. Both nanostripes and free-standing islands are present on the substrate terrace. The step height measured at the free edge of the nanostripes is 1.8 Å, while the height of the islands is 2.0 Å. The greater height of the islands corresponds to a reduced downward contraction of the Cr surface layer, which is due to the greater degree of in-plane relaxation within the islands.

Of course, in-plane relaxation can also occur through the formation of dislocations. However, this is not applicable in the case of Cr/Mo(110), where no dislocations are observed in the nanostripes up to a coverage of 3 ML. This is in contrast to the Fe/Mo(110) system, where dislocation lines appear during the early stages of formation of the second Fe layer and develop into a dislocation network in the third.[4] Since the lattice mismatch for Cr/Mo(110) and Fe/Mo(110) is almost identical, one might expect that the formation of

TABLE I. Interlayer separation calculated using GGA-PBE functionals. The distances are given in Å. The relative changes as compared to the bulk Mo(110) interlayer separation are given in brackets. d_S represents the calculated distance between the surface layer and the layer directly underneath, d_{S-1} represents the distance between this layer and the next underlying layer, and so forth.

	d_S	d_{S-1}	d_{S-2}	d_{S-3}
7 ML Mo(110)	2.133 (−4.1%)	2.248 (+1%)	2.247 (+1%)	
1 ML Cr/Mo(110)	1.887	2.282 (+5.7%)	2.248 (+1%)	2.249 (+1%)
2 ML Cr/Mo(110)	1.609	2.107	2.232 (+0.3%)	2.243 (+0.8%)
1 ML Fe/Mo(110)	1.801	2.274 (+2.2%)	2.244 (+0.8%)	2.247 (+1%)
2 ML Fe/Mo(110)	1.440	2.018	2.229 (+0.2%)	2.244 (+0.8%)

dislocations should occur at around the same coverage in both systems. To understand this behavior, one must compare the interlayer separations calculated for the 2 ML Cr/Mo(110) and 2 ML Fe/Mo(110) slabs, displayed in Table I. The difference in interfacial separation (d_{S-1}) is only 4.4% between the two systems, indicating a similar degree of interfacial bonding. However, the contraction between the first and second layers (d_S) of the Fe bilayer film is 12% larger than that calculated for the Cr bilayer. This indicates that the Fe-Fe bond in the Fe bilayer is stronger than the Cr-Cr bond in the Cr bilayer. The greater stiffness of the Fe film means that maintaining pseudomorphic registry in the 2 ML Fe/Mo(110) system costs more in elastic energy than in the 2 ML Cr/Mo(110) system, which makes the Fe film more susceptible to dislocation formation.

Above 3 ML coverage there is a switch to Stranski-Krastanov growth. Cr films above this coverage are characterized by the formation of three-dimensional wedge-shaped islands like those shown in Fig. 4(a). These islands increase in thickness by one Cr layer for each substrate terrace the island crosses. The formation of three-dimensional islands is driven by the reduction of epitaxial strain, since the islands can partially relieve the epitaxial strain along their free edges.[27,28] The preferential elongation of the islands along the [001] direction may be attributed to either anisotropic diffusion[29] or anisotropic sticking probabilities at island edges.[30] Similar nanowedge islands have been observed for Fe overlayers grown on W(110)[1] and Mo(110),[3,4] as well as for Ni, Cu, and Ho overlayers grown on W(110).[5,31,32] As can be seen in Fig. 4(b), monatomically high steps are present on the (110) surface islands and correspond to incomplete Cr layers on top of the island. The (110) surface of Fe nanowedge islands grown on Mo(110) at a comparable temperature does not display any steps of this kind.[4] The fact that surface energy minimization is more fully achieved in the Fe islands indicates that the mobility of Cr on the surface is lower than that of Fe at these temperatures. In the case of Fe/W(110), the Fe islands were found to be supported on top of a closed pseudomorphic monolayer.[33] For Cr/W(110), it was demonstrated that the islands sit on top of a Cr bilayer, which is thermally stable up to 800 K.[10] Quantitative evaluations of the STM data show that islands in Fig. 4(a) are also supported on a pseudomorphic bilayer.

The morphology and density of the islands is affected by the substrate step orientation and density. This is illustrated in Fig. 4(c), which shows a 4.6 ML film deposited on a region of the Mo(110) surface that has been plastically deformed by the high temperature cleaning procedure. This has resulted in a localized region of a few μm^2 where two step orientations $[\bar{1}11]$ and $[\bar{1}10]$ with different step densities coexist. The islands found on the $[\bar{1}11]$ oriented steps are generally similar to those shown in Fig. 4(a). By comparison, a much lower density of thicker, triangular shaped islands is found on the $[\bar{1}10]$ oriented steps. The influence of step orientation on morphology and magnetic properties has previously been demonstrated for submonolayer growth of Fe on W(110).[34]

The switch to Stranski-Krastanov growth is accompanied by the onset of a two-dimensional dislocation network. Figure 5(a) shows a typical LEED pattern obtained from a multilayer Cr/Mo(110) film, which displays satellite spots characteristic of the lattice distortions produced by the dislocation network. The dislocation network produces a corrugation on the (110) surface of the nanowedge islands as shown in Figs. 5(b) and 5(c). Figure 5(c) illustrates how both the periodicity and amplitude of this corrugation change as a function of the local layer thickness. This behavior is quantified in Figs. 6(a) and 6(b), which plots these parameters as

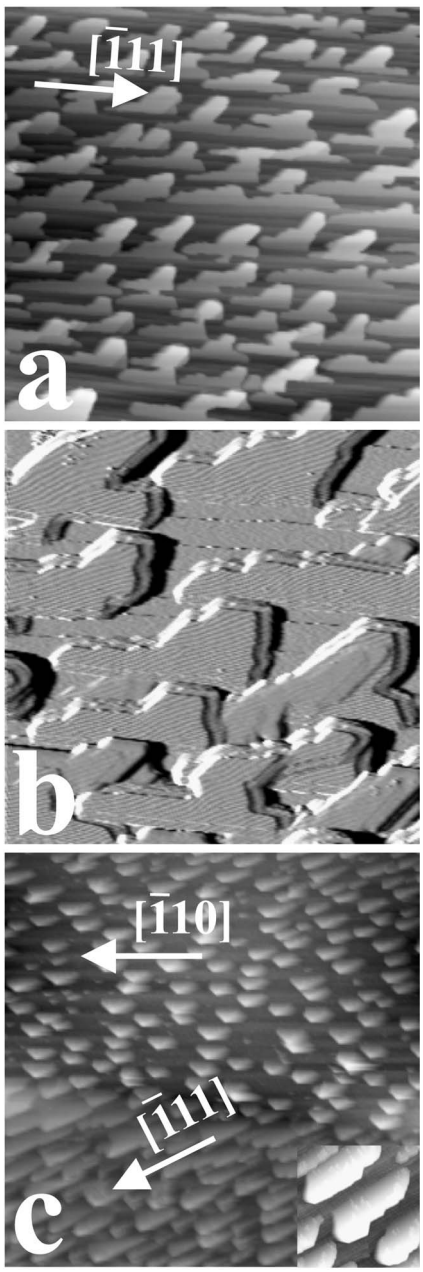

FIG. 4. (a) 1.5×1.5 μm^2 STM image of nanowedge islands formed by the deposition of 3.5 ML on Mo(110) at 575 K. (b) 480×480 nm^2 differentiated image of the same film, showing the monatomic steps between successive layers of the nanowedge islands. (c) 1.5×1.5 μm^2 image of a 5.2 ML film grown at 575 K, showing how the substrate step density and orientation affects the island morphology.

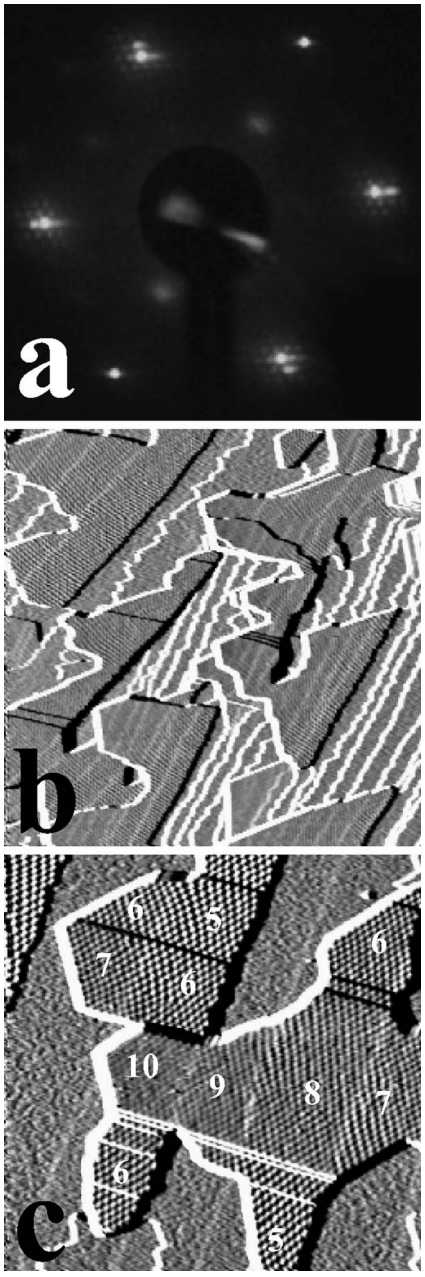

FIG. 5. (a) LEED pattern of a 3 ML Cr film grown on Mo(110) at 575 K, taken with a beam energy $E=118$ eV. (b) 400 $\times 400$ nm^2 differentiated STM image of a 4.0 ML film grown at 575 K. The surface of the islands is broken by monatomic steps (dark lines) and fractional steps (faint lines). The latter follow the position of underlying substrate steps. (c) 173×173 nm^2 differentiated image of the same film, showing how the corrugation and periodicity of the network change with local coverage.

measured from the STM data. It is clear that both the periodicity and amplitude of the corrugation decrease with increasing local thickness. The corrugation amplitude gradually decreases from a maximum value of 1.1 Å at 4 ML to 0.35 Å at 7 ML [Fig. 6(b)]. No corrugation could be resolved above a local thickness of 14 ML. The symmetry of the corrugation pattern also changes with increasing local film thickness. The distortion of the corrugation pattern with respect to the substrate surface is given by the angle γ of the dislocation unit cell highlighted in Fig. 6(c), inset. The angle γ approaches 90° for overlayer thickness higher than 7 ML.

This behavior can be understood in terms of the relaxation of the epitaxial strain. As already mentioned, the first three Cr layers are found to grow pseudomorphically on Mo(110), i.e., the Cr lattice is commensurate with the substrate lattice. At the critical coverage of 4 ML, the elastic energy accumulated as a result of the epitaxial strain exceeds the energy required to form misfit dislocations and the two-dimensional dislocation network is formed at the Cr/Mo(110) interface.[35] The dislocations formed in the first Cr layer release almost all of the epitaxial strain within the overlayer. The remaining epitaxial strain is gradually released in each subsequent layer, i.e., second, third, fourth layers, etc., which maintain a nearly commensurate registry with the underlying layer.[36] The resulting corrugation can be considered as a Moiré pattern which is incommensurate with the substrate lattice.[37] This is demonstrated in Fig. 6(a), where the periodicity measured along the $[1\bar{1}0]$ direction at 4 ML is 61 Å. This corresponds to a factor of 13.7 times the lattice parameter of the Mo(110) surface measured along the $[1\bar{1}0]$ direction. The gradual decrease of the surface corrugation amplitude towards the thicker end of the nanowedge islands shown in Fig. 5(c) is consistent with the idea that the whole dislocation network is buried at the same depth in the island. The corrugation amplitude decreases with increasing thickness as the first Cr layer in which the dislocations are formed is buried by subsequent layers.

The change in the in-plane epitaxial strain described above produces a corresponding change in the out-of-plane tetragonal distortion of the Cr layers. This is illustrated in Fig. 6(d), which plots the average interlayer distance within the Cr islands as a function of local thickness. As the tensile epitaxial strain is relieved, the out-of-plane contraction of the Cr multilayer is lowered, giving rise to a higher average interlayer separation. As a result, fractional steps are observed at the position of buried substrate steps [cf. Fig. 5(b)], at the point where the island becomes one layer thicker and the strain state changes by some amount. These fractional steps were not observed in previous STM studies of Fe/Mo(110) nanowedge islands,[4] though the positions of buried substrate steps were distinguished in Fe/W(110) nanowedge islands.[1] The height of these fractional steps is greatest at the thin edge of the islands and decreases to zero towards their thick end. We have measured fractional step heights on top of the islands of 0.35 Å between 4 and 5 ML local coverage, 0.25 Å between 5 and 6 ML, and 0.15 Å between 6 and 7 ML.

IV. CONCLUSIONS

The elevated temperature growth of Cr on Mo(110) has been studied using STM and LEED. The Cr films form pseudomorphic nanostripes by the step-flow growth mechanism up to a coverage of 3 ML. Above this coverage, there is a switch to Stranski-Krastanov growth with the formation

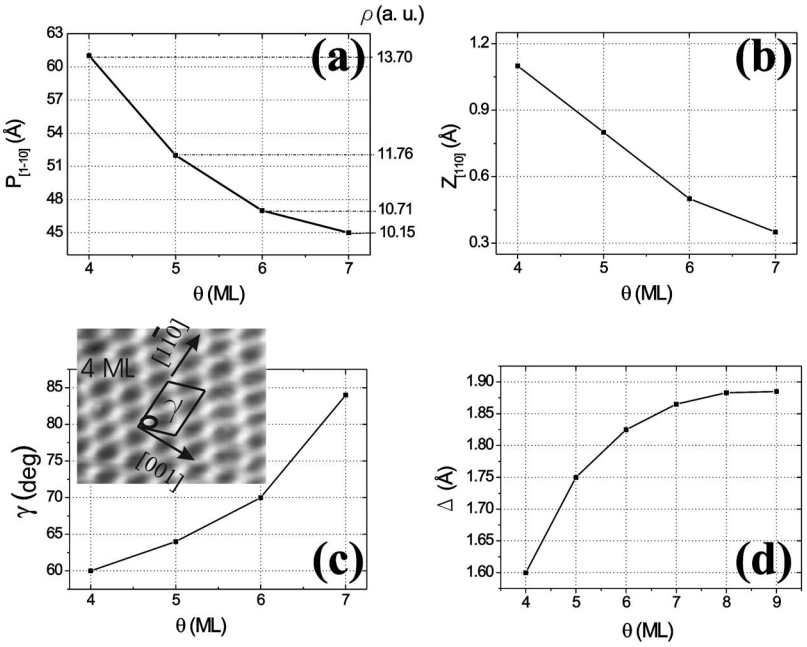

FIG. 6. (a) Periodicity and (b) amplitude of the corrugation measured on top of the Cr nanowedge islands as a function of local layer thickness. The parameter ρ on the right side of (a) is the ratio between the corrugation periodicity along the $[1\bar{1}0]$ direction and the corresponding atomic periodicity of the Mo(110) surface (4.4505 Å). (c) Symmetry change of the corrugation pattern as a function of local thickness. The unit cell and angle γ are highlighted in the inset. (d) Average Cr interlayer spacing Δ measured as a function of local film thickness.

of Cr nanowedge islands. This is accompanied by the formation of a two-dimensional dislocation network within the islands. Using DFT calculations, we have compared the multilayer relaxation of the Cr/Mo(110) and Fe/Mo(110) epitaxial interfaces. We conclude that the Cr films have a lower stiffness than their Fe counterparts, which makes them more stable against dislocation formation despite a comparable lattice mismatch. The multilayer relaxation of the surface is responsible for the fractional steps observed between successive Cr layers and changes as the in-plane strain is gradually released.

ACKNOWLEDGMENT

This work was supported by Science Foundation of Ireland (SFI) under Contract 00/PI.1/C042.

*Corresponding author. Fax: +353-1-608-3228; Email address: casacua@tcd.ie

[1] H. Bethge, D. Heuer, C. Jensen, K. Reshöft, and U. Köhler, Surf. Sci. **331-333**, 878 (1995).
[2] W. Wulfhekel, F. Zavaliche, F. Porrath, H. Oepen, and J. Kirschner, Europhys. Lett. **49**, 651 (2000).
[3] J. Malzbender, M. Przybylski, J. Giergiel, and J. Kirschner, Surf. Sci. **414**, 187 (1998).
[4] S. Murphy, D. MacMathúna, G. Mariotto, and I. V. Shvets, Phys. Rev. B **66**, 195417 (2002).
[5] C. Schmidthals, D. Sander, A. Enders, and J. Kirschner, Surf. Sci. **417**, 361 (1998).
[6] W. Wulfhekel, T. Gutjahr-Löser, F. Zavaliche, D. Sander, and J. Kirschner, Phys. Rev. B **64**, 144422 (2001).
[7] M. Pratzer and H. Elmers, Surf. Sci. **550**, 223 (2004).
[8] A. Mikkelsen, L. Ouattara, and E. Lundgren, Surf. Sci. **557**, 109 (2004).
[9] A. Melmed and N. Shinn, Surf. Sci. **193**, 475 (1988).
[10] P. Berlowitz and N. Shinn, Surf. Sci. **209**, 345 (1989).
[11] U. Gradmann and G. Waller, Surf. Sci. **116**, 539 (1982).
[12] E. -P. Kim, T. -H. Kim, S.-T. Kim, Y. Kuk, and S.-J. Kahng, Thin Solid Films **441**, 317 (2003).
[13] A. M. N. Niklasson, J. M. Wills, and L. Nordström, Phys. Rev. B **63**, 104417 (2001).
[14] A. Kubetzka, M. Bode, O. Pietzsch, and R. Wiesendanger, Phys. Rev. Lett. **88**, 057201 (2002).
[15] L. Vitos, A. Ruban, H. Skriver, and J. Kollár, Surf. Sci. **411**, 186 (1998).
[16] M. Segall, P. Lindan, M. Probert, C. Pickard, P. Hasnip, S. Clark, and M. Payne, J. Phys.: Condens. Matter **14**, 2717 (2002).
[17] J. P. Perdew, K. Burke, and M. Ernzerhof, Phys. Rev. Lett. **77**, 3865 (1996).
[18] G. S. Bales and A. Zangwill, Phys. Rev. B **41**, 5500 (1990).
[19] G. Ehrlich and F. Hudda, J. Chem. Phys. **44**, 1039 (1966).
[20] R. Schwoebel and E. Shipsey, J. Appl. Phys. **37**, 3682 (1966).
[21] A. Li, F. Liu, D. Y. Petrovykh, J.-L. Lin, J. Viernow, F. J. Himpsel, and M. G. Lagally, Phys. Rev. Lett. **85**, 5380 (2000).
[22] S. Murphy, G. Mariotto, N. Berdunov, and I. V. Shvets, Phys. Rev. B **68**, 165419 (2003).
[23] H. J. Elmers, J. Hauschild, H. Höche, U. Gradmann, H. Bethge, D. Heuer, and U. Köhler, Phys. Rev. Lett. **73**, 898 (1994).
[24] M. Arnold, S. Sologub, G. Hupfauer, P. Bayer, W. Frie, L. Hammer, and K. Heinz, Surf. Rev. Lett. **4**, 1291 (1997).
[25] L. M. de la Garza and L. Clarke, J. Phys. C **14**, 5391 (1981).
[26] X. Qian, F. Wagner, M. Petersen, and W. Hübner, J. Magn. Magn. Mater. **213**, 12 (2000).
[27] B. Orr, D. Kessler, D. Snyder, and L. Sander, Europhys. Lett. **19**, 32 (1992).

[28] P. Müller and R. Kern, Surf. Sci. **457**, 229 (2000).
[29] U. Köhler, C. Jensen, C. Wolf, A. Schindler, L. Brendel, and D. Wolf, Surf. Sci. **454-456**, 676 (2000).
[30] M. Albrecht, M. Fritzsche, and U. Gradmann, Surf. Sci. **294**, 1 (1993).
[31] K. Reshöft, C. Jensen, and U. Köhler, Surf. Sci. **421**, 320 (1999).
[32] G. Piaszenski, R. Göbel, C. Jensen, and U. Köhler, Surf. Sci. **454-456**, 712 (2000).
[33] D. Sander, A. Enders, C. Schmidthals, D. Reuter, and J. Kirschner, J. Magn. Magn. Mater. **177-181**, 1299 (1998).
[34] H. Elmers, J. Hauschild, and U. Gradmann, J. Magn. Magn. Mater. **221**, 219 (2000).
[35] C. Günther, J. Vrijmoeth, R. Q. Hwang, and R. J. Behm, Phys. Rev. Lett. **74**, 754 (1995).
[36] R. Popescu, H. L. Meyerheim, D. Sander, J. Kirschner, P. Steadman, O. Robach, and S. Ferrer, Phys. Rev. B **68**, 155421 (2003).
[37] H. Brune, H. Röder, C. Boragno, and K. Kern, Phys. Rev. B **49**, 2997 (1994).